Journal of Alloys and Compounds 509 (2011) 9869–9875

Contents lists available at ScienceDirect

Journal of Alloys and Compounds

journal homepage: www.elsevier.com/locate/jallcom

Effect of oxide shells on the magnetic and magnetotransport characteristics of oxidized FeCoZr nanogranules in Al_2O_3

J. Fedotova[a,*], J. Kasiuk[a], J. Przewoznik[b], Cz. Kapusta[b], I. Svito[c], Yu. Kalinin[d], A. Sitnikov[d]

[a] NC PHEP BSU, 220040 Minsk, Belarus
[b] AGH University of Science and Technology, Faculty of Physics and Applied Computer Science, Department of Solid State Physics, 30-059 Krakow, Poland
[c] Belarusian State University, 220030 Minsk, Belarus
[d] Voronez State Technical University, 394026 Voronez, Russia

ARTICLE INFO

Article history:
Received 22 October 2010
Received in revised form 19 July 2011
Accepted 21 July 2011
Available online 2 August 2011

Keywords:
Magnetic properties in films
Surfaces and interfaces
Magnetotransport phenomena
Materials for magnetotransport
Fine-particle systems
Nanocrystalline materials

ABSTRACT

The paper reports on the results of a comparative study of magnetic and magnetotransport properties of granular nanocomposite films FeCoZr–Al_2O_3 synthesized in pure Ar and Ar + O sputtering atmosphere. Effects of oxygen incorporation on the temperature and magnetic field dependencies of magnetization and electrical resistance of the films are discussed with respect to the "core–shell" structure formation. Peculiarities of coercive force variation with temperature are analyzed and discussed.

1. Introduction

Nanocomposites containing nanogranules of ferromagnetic alloy (such as FeCo, FeNi, etc.) in dielectric matrix (SiO_2, Al_2O_3, etc.) could be applied for designing various magnetoelectronic devices (sensors) to be utilized at high frequencies [1–3]. The industrial importance of such materials is related to the optimal combination of relatively high electrical resistivity ρ, low values of coercive field H_C and high magnetoresistivity values ($MR = \Delta\rho/\rho = (\rho_{H\neq 0} - \rho_{H=0})/\rho_{H=0}$). The ratio between metallic and dielectric fractions, magnetic structure of nanogranules, properties of the interface between nanogranules and matrix are among the most important factors influencing ρ, H_C and $\Delta\rho/\rho$ in granular nanocomposites. In the context of MR effect enhancement films composition within the onset of percolative cluster formation is the most promising [4]. The peculiarity of this composition is that the thickness of dielectric barriers between granules is minimal, but metallic conductivity paths are not formed yet. Apart from structural features, as mentioned above, the important role in MR value is played by the interface between metallic nanogranules and matrix. It is particularly evident when metallic nanoparticles are covered with oxide shell and the "ferromagnetic core–oxide shell" structure is formed inside the matrix. The enhancement of *MR* effect related to the spin-dependent tunneling in "core–shell" structures was previously reported in [5] for Co–CoO system. A homogeneous size distribution of Co cores and CoO shells was considered as the origin of MR enhancement in this case.

Variations of magnetization M(H) and coercive field H_C quite commonly observed in "core–shell" structures due to ferromagnetic–antiferromagnetic (FM-AMF) (or ferromagnetic–ferrimagnetic) coupling between core and shell [5–7] should be considered as well.

Actually, the formation of "core–shell" structures originates from either undesirable oxygen deposition on the particle–matrix interface or intentional synthesis of granular film in oxygen-containing sputtering atmosphere. The latter approach is usually applied for some specific combinations of granules and matrix materials when passivation with oxygen is the only technological opportunity to stabilize granular nanostructure of composite materials.

Recent study of granular nanocomposites $(FeCoZr)_x(Al_2O_3)_{100-x}$ (17 at. % $\leq x \leq$ 65 at. %) by means of room-temperature transmission ^{57}Fe Mössbauer spectroscopy revealed that the formation of "core-shell" structure could occur in these materials due to the synthesis in oxygen-containing sputtering atmosphere [8,9]. Mössbauer spectra in this case were successfully simulated with the assumption that granules contain the superparamagnetic core of soft ferromagnetic FeCoZr alloy inside the shell constituting the

* Corresponding author.
E-mail address: julia@hep.by (J. Fedotova).

0925-8388/$ – see front matter © 2011 Elsevier B.V. All rights reserved.
doi:10.1016/j.jallcom.2011.07.066

superposition of $(Fe^{3+})Co$ superparamagnetic oxide and paramagnetic $(Fe^{2+})Co$ oxide. It was established that the quantitative ratio between core and shell as well as the fractions of $(Fe^{3+})Co$ and $(Fe^{2+})Co$ was depending on x [8,9].

Thus, granular nanocomposites sintered in oxygen-containing atmosphere should be considered as an appropriate object for the investigation of FeCo-oxide shells effect on the magnetic characteristics of FeCoZr granules and also on the magnetoresistance of nanocomposites as a whole. On the other hand, a consistent analysis of temperature T and field H dependencies of magnetization and magnetoresistance is the way to verify the picture of "core–shell" structure formed on the basis of transmission Mössbauer spectroscopy results.

2. Experimental

Granular nanocomposite films $(Fe_{45}Co_{45}Zr_{10})_x(Al_2O_3)_{100-x}$ (36 at.% $\leq x \leq$ 64 at.%) were synthesized by ion-beam sputtering of complex target (containing Al_2O_3 strips on FeCoZr substrate [10]) in oxygen-free ($P_{Ar} = 6.7 \times 10^{-2}$ Pa) and oxygen-containing sputtering atmosphere onto glass–ceramic and Al substrates ($P_{Ar+O} = 9.6 \times 10^{-2}$ Pa, $P_O = 4.2 \times 10^{-3}$ Pa).

The composition of FeCoZr alloy nanogranules and the ratio between metallic and dielectric fractions in the films were confirmed to be close to nominal, by energy dispersive X-ray spectroscopy (EDX) in a scanning electron microscope and by Rutherford backscattering spectrometry (RBS) with experimental errors of 1 at.% and 0.1 at.% respectively [8,10]. The analysis of morphology in the granular films studied with the transmission electron microscopy (TEM) revealed typical granular structure with metallic nanoparticles of medium size ranging between 2 and 7 nm. Recent experiments on X-ray and electron diffraction revealed broadened reflections related to a considerable disorder in the bcc-FeCo-based structure or a small size of nanogranules [11].

Compositions of granular films sintered in oxygen-free atmosphere were chosen with respect to their electrical conductivity [12] and results of Mössbauer spectroscopy [8,9]. Selected samples $(FeCoZr)_{42}(Al_2O_3)_{58}$, $(FeCoZr)_{47}(Al_2O_3)_{53}$ and $(FeCoZr)_{50}(Al_2O_3)_{50}$ correspond to compositions below percolation, within percolation threshold X_C and above percolation, respectively. In oxygen-containing samples Mössbauer spectroscopy revealed partial oxidation of FeCoZr nanoparticles and formation $(Fe^{3+})Co$- and $(Fe^{2+})Co$-oxides [8,9]. So that the compositions $(FeCoZr)_{35}(Al_2O_3)_{65}$, $(FeCoZr)_{56}(Al_2O_3)_{44}$, $(FeCoZr)_{59}(Al_2O_3)_{41}$ were selected to cover different ratios between metallic and dielectric fractions.

Magnetization of samples $M(H)$ was studied with Quantum Design VSM-PPMS in the temperature range 2–300 K in magnetic fields H up to 89 kOe. Temperature dependencies of samples magnetization $M(T)$were measured in field-cooled (FC, $H = 50$ Oe) and zero field-cooled (ZFC) regimes. All the $M(H)$ curves discussed below are presented after extraction of glass–ceramic and Al_2O_3 contributions. Resulting magnetizations were normalized to the mass of FeCoZr particles, i.e. M^{mass} is mass magnetization of FeCoZr particles.

Magnetoresistivity MR of the samples was measured with four-probe method in closed-cycle cryostat at the temperature 300 K in magnetic fields H up to 80 kOe.

3. Results

3.1. Magnetometry of granular films FeCoZr-Al_2O_3

Magnetization as a function of temperature, $M(T)$, recorded in FC and ZFC modes on the samples synthesized in oxygen are presented in Fig. 1d–f. The curves are much different from $M(T)$ dependencies that were observed for non-oxidized granular films [13]. These curves are shown in Fig. 1a–c for comparison. As evidenced from Fig. 1, films sintered in oxygen-containing atmosphere reveal generally lower blocking temperatures T_B, defined as the maximum of ZFC curves. One should also note that for this particular case almost no discrepancy is observed between T_B and bifurcation temperature T_b. Considering relatively broad size distribution of nanogranules derived from Mössbauer spectroscopy [8,9], magnetometry, etc., T_B should be regarded as a characteristics of some average "core–shell" nanogranule. The abovementioned peculiarities of T_B and T_b values may be assigned to a much narrower size distribution of oxidized FeCoZr nanogranules as compared to oxygen-free samples.

The granular film of $(FeCoZr)_{35}(Al_2O_3)_{65}$ composition shows a steep decrease of M with increasing temperature in the FC mode

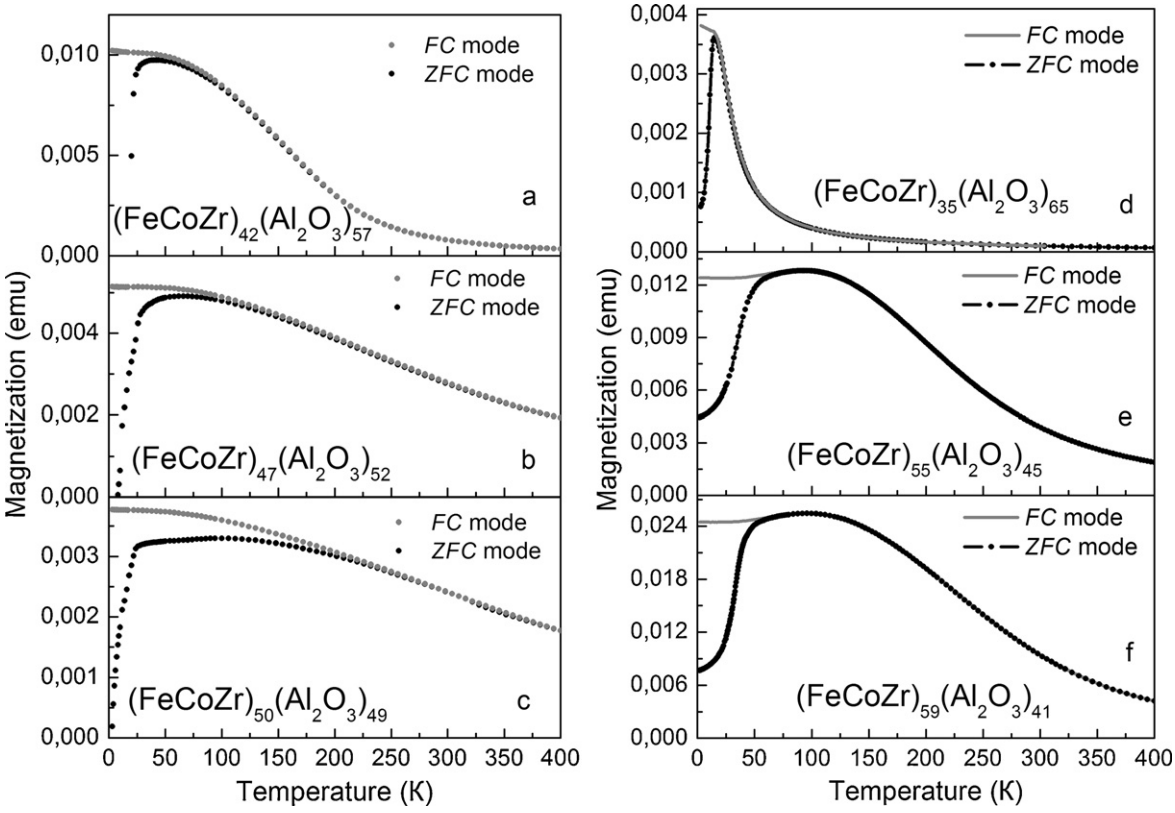

Fig. 1. Temperature dependencies of magnetization $M(T)$, recorded in FC and ZFC modes ($H = 50$ Oe) for granular films sintered in oxygen-free (a–c) and oxygen-containing (d–f) sputtering atmosphere.

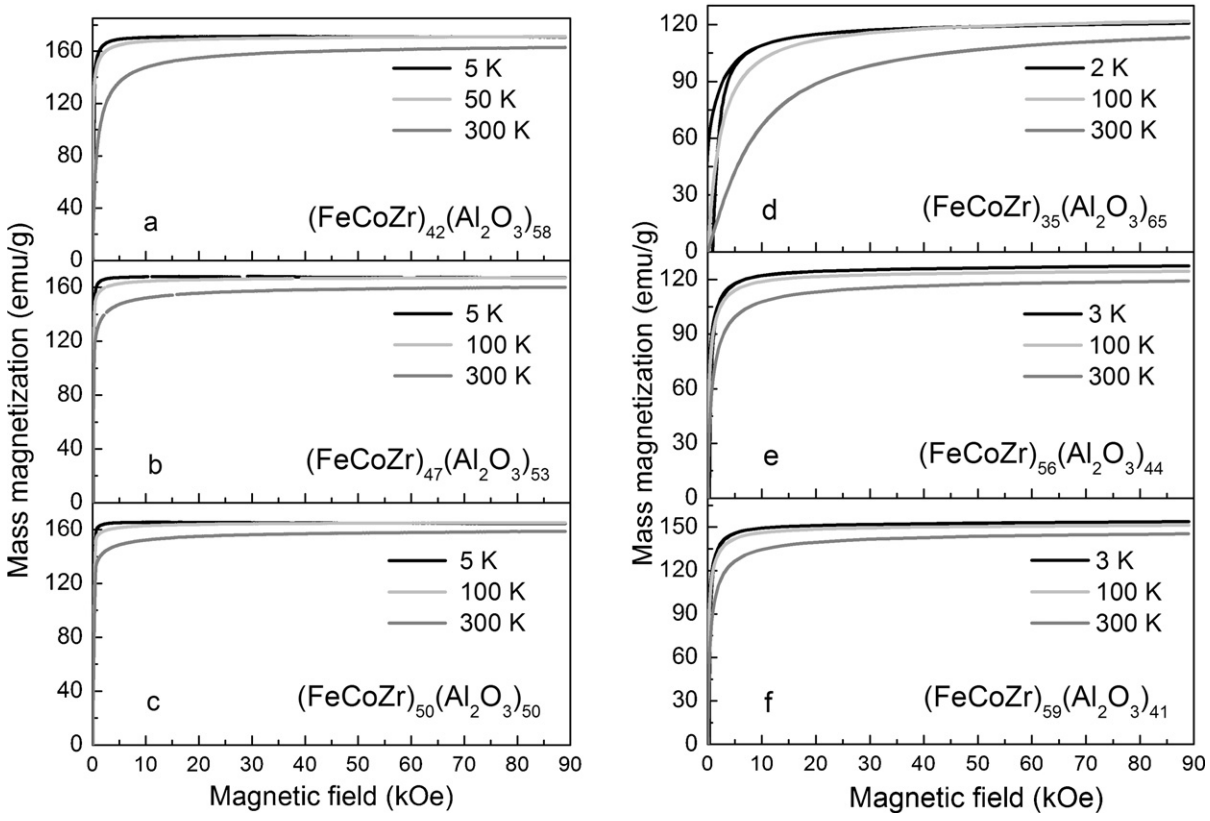

Fig. 2. Field dependencies of mass magnetization $M^{mass}(H)$ for selected samples $(FeCoZr)_x(Al_2O_3)_{100-x}$, sintered in oxygen-free (a–c) and oxygen-containing (d–f) sputtering atmosphere.

that corresponds to temperature-induced disordering of magnetic moments of non-interacting superparamagnetic nanoparticles.

In contrast to the $(FeCoZr)_{35}(Al_2O_3)_{65}$ case, magnetization curves versus temperature recorded in the FC regime for oxidized films $(FeCoZr)_{56}(Al_2O_3)_{44}$ and $(FeCoZr)_{59}(Al_2O_3)_{41}$, are almost constant up to about 93 K and 96 K, respectively (see Fig. 1e and f). Both temperatures correspond to flat maxima of ZFC magnetization curves for mentioned compositions and should be assigned to T_B values for ensembles of different nanoparticles.

Field dependencies of mass magnetization (first quadrants of magnetization loops) $M^{mass}(H)$ for the samples $(FeCoZr)_x(Al_2O_3)_{100-x}$, sintered in oxygen-free and oxygen-containing sputtering atmosphere are shown in Fig. 2a–c and d–f respectively. $M^{mass}(H)$ curves obtained for non-oxidized granular films reveal relatively small saturation fields $H_S \sim 4$–10 kOe and close to zero coercive field H_C even when measured at 5 K. Such features are typical for magnetically soft amorphous FeCoZr nanoparticles. Values of saturation mass magnetization M_S^{mass} for different compositions are close to 170 emu/g at 5 K and slightly decrease with increasing T_{mes} up to 300 K. So that the magnetic moment per average $Fe_{50}Co_{50}$ atom ($\mu_S \approx 2\,\mu_B$ for $(FeCoZr)_{50}(Al_2O_3)_{50}$) derived from experimental data is lower than for bulk bcc FeCo alloy ($\mu_S = 2.4\,\mu_B$ for $Fe_{50}Co_{50}$ [14]) that is a signature of disordered structure and a small size of FeCoZr granules.

In contrast to oxygen-free films, $M^{mass}(H)$ curves of samples sintered in oxygen-containing atmosphere were unsaturated for all the studied compositions at 300 K (see Fig. 2d–f). For $(FeCoZr)_{35}(Al_2O_3)_{65}$ the mass magnetization does not achieve saturation even at 2 K. Such a behavior is typical for the ensembles of isolated superparamagnetic nanoparticles. Fig. 2d–f reveals also some increase of mass magnetization with decreasing T that is usual for amorphous ferromagnetics and is related to a decreasing influence of thermal energy.

Table 1
Saturation mass magnetization M_S^{mass} (or mass magnetization at maximum magnetic field $H_{max} = 89$ kOe) per $Fe_{45}Co_{45}Zr_{10}$ (emu/g) and blocking temperature T_B (K).

Composition	Temperature of measurement (K)					Blocking temperature T_B (K)
	5	50		100	300	
Synthesis in oxygen-free sputtering atmosphere						
$(FeCoZr)_{42}(Al_2O_3)_{58}$	171	171		–	163	45
$(FeCoZr)_{47}(Al_2O_3)_{53}$	167	–		167	160	65
$(FeCoZr)_{50}(Al_2O_3)_{50}$	165	–		165	159	105
Synthesis in oxygen-containing sputtering atmosphere						
	2	3	50	100	300	
$(FeCoZr)_{35}(Al_2O_3)_{65}$	121	–	115	122	113	16
$(FeCoZr)_{56}(Al_2O_3)_{44}$	–	127	–	125	119	93
$(FeCoZr)_{59}(Al_2O_3)_{41}$	–	154	153	151	146	96

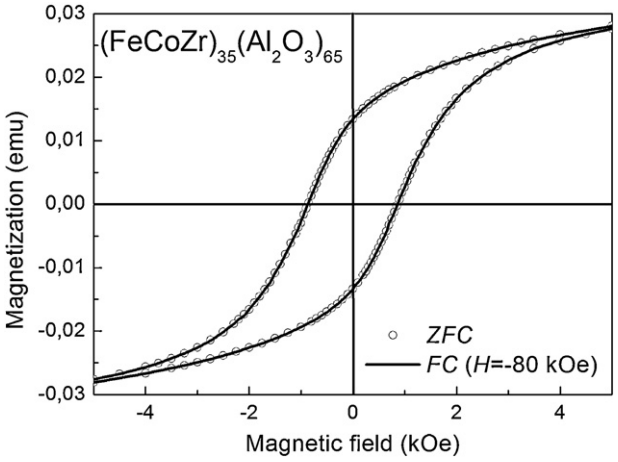

Fig. 3. $M(H)$ dependencies measured at 2 K with ZFC and FC procedures (at $H = 80$ kOe) for composition $(FeCoZr)_{35}(Al_2O_3)_{65}$.

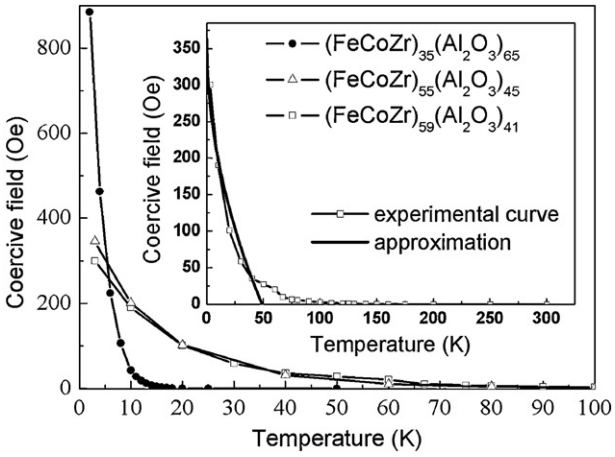

Fig. 4. Temperature dependencies of coercive field H_C of FeCoZr-Al_2O_3 sputtered in oxygen-containing atmosphere. The inset shows temperature dependence of coercive field H_C for granular film $(FeCoZr)_{59}(Al_2O_3)_{41}$, together with its approximation.

It should be emphasized that oxidized nanoparticles generally exhibit lower M_S^{mass} values as compared with granular films sintered in oxygen-free atmosphere (see Table 1). It is noteworthy that M_S^{mass} values are much higher than those for iron oxides or cobalt ferrites [15,16]. This suggests a partial oxidation of FeCoZr nanoparticles, that is supported with earlier results of Mössbauer spectroscopy [8]. One should note that M_S^{mass} values for non-oxidized and oxidized granular films summarized in the Table 1 are normalized per mass of the FeCoZr alloy or oxidized FeCoZr alloy. A correction of M_S^{mass} due to mass contributions of zirconium and oxygen is small and not important for further consideration.

One of the methods to verify the presence of FM-AFM "core–shell" coupling in nanostructures is to compare magnetization curves measured *vs* applied field at a temperature much below T_B after ZFC and FC (at $H = 80$ kOe) procedures. Such an experiment was performed on the film with composition $(FeCoZr)_{35}(Al_2O_3)_{65}$. The typical feature of FM-AFM coupling between ferromagnetic core and oxide shell is a shift of the $M(H)$ curve measured after *field-cooling* with respect to that measured after zero field cooling. The shift of hysteresis loop is often accompanied with an enhancement of H_C values observed after FC procedure. $M(H)$ curves obtained in both regimes are presented in Fig. 3. One can see that both $M(H)$curves fully coincide making clear that no noticeable FM–AFM coupling (exchange bias) occurs between core and shell, Neel temperature is greater than 300 K or oxide shell is ferromagnetic.

Temperature dependencies of H_C should also be analyzed in the context of a possible "core–shell" structure. $H_C(T)$ dependencies for selected films compositions are shown in Fig. 4.

Fig. 4 reveals that for all analyzed compositions H_C values decrease with growing temperature T and tend towards zero value at T_B. Such a behavior is typical for the assembly of superparamagnetic nanogranules. According to the theory, temperature dependence of H_C for sample containing single-domain granules of equal size follows the relationship [17]:(1)$H_C = H_{C_0}\left[1 - \left(\frac{T}{T_B}\right)^{1/2}\right]$, where H_{C_0} is H_C of the sample at $T = 0$ K.

H_{C_0} is the magnetic field necessary for remagnetization of single-domain spherical particle by means of coherent rotation and is defined with the formulae [17]:(2)$H_{C_0} = \frac{2\alpha K_{eff}}{M_S}$, where K_{eff} – effective anisotropy constant, M_S – saturation magnetization, α – phenomenological constant. For $(FeCoZr)_{59}(Al_2O_3)_{41}$ $H_{C_0} = 364$ Oe.

Approximation of experimental $H_C(T)$ for the sample $(FeCoZr)_{59}(Al_2O_3)_{41}$ assuming this formula (see the inset in Fig. 4) provides T_B equal to 49 K which does not coincide with T_B value (96 K) determined from maximum of ZFC curve (see Fig. 1f). The discrepancy between the approximation and the experimental curve as well as the inconsistency of T_B values seems to be due to broad distribution of nanoparticles sizes.

In order to obtain a better approximation of experimental data $H_C(T)$ curves were re-plotted in logarithmic scale and presented in Fig. 5. One can see that experimental curves could be successfully fitted with the empirical dependence $y = a - bT^{\alpha}$ which is different from Eq. (1). The main purpose for this approximation is a precise definition of T_{SP} that separates superparamagnetic state from magnetically ordered one. It is worth noting that experimental curve nicely follows nearly linear fit up to the 0.2 Oe level, with α values of 1.44(6), 0.87(2) and 0.80(3) for $x = 35$, 55 and 59, respectively. The value of α slightly lower than 1 is observed for the samples with large x, whereas it is much larger than 1 for $x = 35$. H_C value of 0.2 Oe can be considered as a reasonable measure of the experimental error of H_C determination. The intersections of linear approximation with temperature axis provide the T_{SP} values where H_C becomes zero, i.e., the temperatures where overwhelming majority of oxidized FeCoZr nanoparticles become superparamagnetic. One should note that extracted T_{SP} values do not coincide with T_B values (shown with dashed lines in Fig. 5) evidencing broad size distribution of nanogranules. The coincidence between T_{SP} and T_B is improving with the decrease of FeCoZr fraction confirming narrower size distribution of nanogranules in the $(FeCoZr)_{35}(Al_2O_3)_{65}$ film.

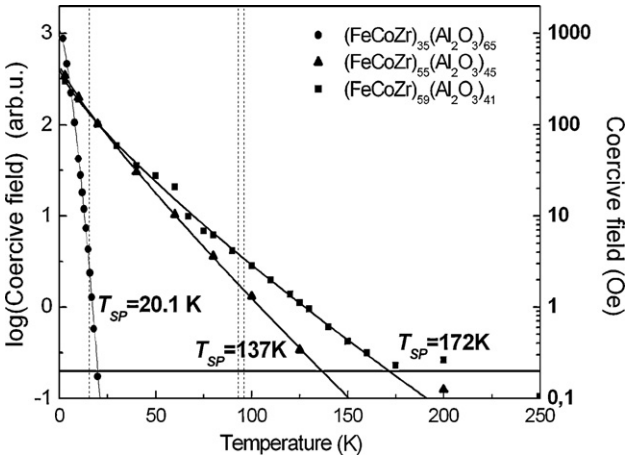

Fig. 5. Approximation of temperature dependencies of coercive field H_C (in logarithmic scale) of FeCoZr-Al_2O_3 synthesized in oxygen-containing sputtering atmosphere. Dashed lines correspond to blocking temperatures T_B (see Fig. 1).

Table 2
Parameters of selected oxygen-containing granular films FeCoZr-Al_2O_3.

Composition	Curie–Weiss temperature θ_{CW} (K)	Volume of nanoparticle V (nm^3)	Size of nanoparticle d (nm)
$(FeCoZr)_{35}(Al_2O_3)_{65}$	83	9	2.5
$(FeCoZr)_{56}(Al_2O_3)_{44}$	221	64	4.9
$(FeCoZr)_{59}(Al_2O_3)_{41}$	245	98	5.7

Values of T_B and, consequently, the size (diameter) of nanogranules d for oxygen-containing granular films generally seem to be lower than those for oxygen-free samples (see Table 1). Nanoparticles size can be determined by the application of Curie–Weiss law to the relationship between magnetic susceptibility χ and Curie–Weiss temperature [17]. By modification of this law the volume V of superparamagnetic nanoparticle can be expressed as:(3)$V = \frac{3k_B(T-\theta_{CW})\chi_{mass}(T)}{\mu_0(M_S^{mass})^2\rho}$,where k_B – Boltzmann constant, $\chi_{mass} = \chi/m_{FeCoZr}$ – mass magnetic susceptibility of FeCoZr nanoparticles (magnetic susceptibility of sample divided by mass of FeCoZr nanoparticles), θ_{CW} – Curie–Weiss temperature, μ_0 – magnetic permeability of vacuum, M_S^{mass} – mass magnetization of FeCoZr nanoparticles at H_{max}, ρ – density of FeCoZr nanoparticles.

The magnetic susceptibility of the samples χ_{mass} at 300 K was determined from the slope of linear part of $M(H)$ curve at zero H values. Values of θ_{CW} were extracted from the intersection with temperature axis of linear approximation of reciprocal $M(T)$ curve (proportional to χ_{mass} (T)) obtained at external fields closest to zero. Values of θ_{CW}, V and d for the $(FeCoZr)_{35}(Al_2O_3)_{65}$, $(FeCoZr)_{56}(Al_2O_3)_{44}$ and $(FeCoZr)_{59}(Al_2O_3)_{41}$ films are summarized in the Table 2.

It is worth noting that the estimation of the volume for complex "core–shell" nanogranules assuming simple relationship $25k_BT_B = KV$ (where k_B – Boltzmann constant, K – magnetic anisotropy constant, V – volume of nanoparticle) [18] is not fully correct.

In this case nanogranules size should rather be defined by approximation of $M(H)$ curves with Langevin function. This is appropriate for considered case of the system (ensemble) containing non-interacting superparamagnetic nanogranules. Approximation was performed on the $M(H)$ curve recorded for the $(FeCoZr)_{59}(Al_2O_3)_{41}$ film. For this particular composition dominating contribution of superparamagnetic $(Fe^{3+})Co$ oxide was proved by Mössbauer spectroscopy [8,9]. Assuming a log-normal size distribution of nanoparticles the dependence of the magnetization on H is fitted with the following expression:(4)$M^{vol}(H) = M_S^{vol}\int_0^\infty \left[L(\frac{M_S^{vol}VH}{k_BT})\right] f(V)dV$,where $L(x) = \mathrm{cth}(x) - 1/x$ – Langevin function, $f(V) = 1/\sqrt{2\pi\sigma}V\exp\left[-\ln^2(V/\langle V\rangle)/2\sigma^2\right]$ – log-normal size distribution of nanoparticle, $\langle V\rangle$ and σ – distribution parameters (mediana and width, respectively), M_S^{vol} – volume saturation magnetization of nanogranules. For the $(FeCoZr)_{59}(Al_2O_3)_{41}$ film the value of metallic particles magnetization at H_{max} = 89 kOe (1021 emu/cm^3) is regarded as M_S^{vol}.

The result of the approximation is shown in Fig. 6.

The best fit of the experimental $M^{vol}(H)$ curve is obtained for parameters $\langle V\rangle$ and σ of 145 nm^3 and 1.5, respectively. Size distribution of oxidized "core–shell" nanogranules derived from fitting is shown in the inset to the Fig. 6. Assuming spherical shape of nanogranules and the relationship $\langle V\rangle = \pi\cdot\langle d\rangle^3/6$, the corresponding average diameter $\langle d\rangle$ is estimated to be 6.5 nm. It is interesting to note that the peak of distribution function corresponds to nanogranules of 3.1 nm in size while about 10% of nanogranules appears to be larger than 12.5 nm.

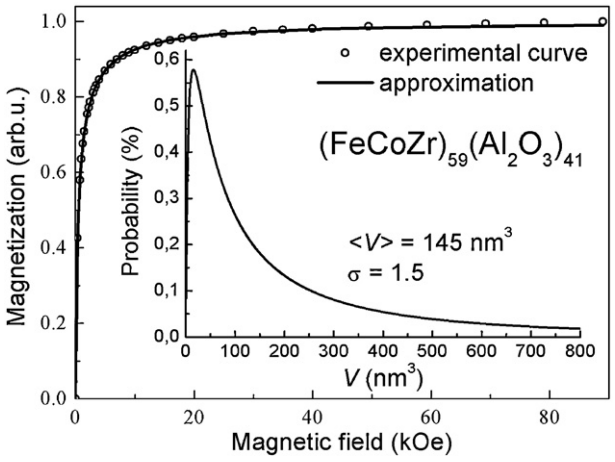

Fig. 6. The approximation of the experimental $M^{vol}(H)$curve recorded on $(FeCoZr)_{59}(Al_2O_3)_{41}$ granular film at 300 K with Langevin function. The inset shows size distribution of oxidized "core–shell" nanogranules derived from fitting.

It is noteworthy that the attempt for similar approximation of the $M^{vol}(H)$ curve recorded on the $(FeCoZr)_{35}(Al_2O_3)_{65}$ film was unsuccessful, possibly due to more complex "core-shell" structure.

3.2. Correlation between magnetoresistivity and magnetization of FeCoZr-Al_2O_3

It was reported in [19] that for granular nanocomposites exhibiting spin-dependent tunneling magnetoresistivity $\Delta\rho/\rho$ is proportional to the squared normalized magnetization $-(M(H)/M_S)^2$. Obviously, magnetotransport in FeCoZr-Al_2O_3 granular films should follow the mechanism of spin-dependent tunneling for compositions below percolation limit, that is when films constitute the ensemble of superparamagnetic nanogranules isolated in the matrix e.g. due to the oxide shell formation. Thus, the correspondence between $\Delta\rho/\rho$ and $-(M(H)/M_S)^2$ curves should support the "core–shell" structure of nanogranules in oxidized FeCoZr-Al_2O_3 granular films.

Fig. 7 shows room temperature $\Delta\rho/\rho$ and $-(M(H)/M_S)^2$ curves for $(FeCoZr)_{42}(Al_2O_3)_{58}$ and $(FeCoZr)_{47}(Al_2O_3)_{53}$ films synthesized in oxygen-free sputtering atmosphere, and $(FeCoZr)_{55}(Al_2O_3)_{45}$ and $(FeCoZr)_{59}(Al_2O_3)_{41}$ films prepared in oxygen-containing atmosphere. It is clear (see Fig. 7 a) that excellent correlation between $\Delta\rho/\rho$ and $-(M(H)/M_S)^2$ occurs for oxygen-free films before percolation, particularly for the composition $(FeCoZr)_{42}(Al_2O_3)_{58}$. At percolation configuration represented by the $(FeCoZr)_{47}(Al_2O_3)_{53}$ sample the discrepancy between the two curves is pronounced and the value of $\Delta\rho/\rho$ is much lower than for $(FeCoZr)_{42}(Al_2O_3)_{58}$ reflecting the formation of current-conductive paths between the FeCoZr nanogranules (see Fig. 7 b).

In contrast to the expectations, a good coincidence of $\Delta\rho/\rho$ and $-(M(H)/M_S)^2$ is found for oxygen-containing films $(FeCoZr)_{55}(Al_2O_3)_{45}$ and $(FeCoZr)_{59}(Al_2O_3)_{41}$, i.e. at the concentration of oxidized metallic granules above the percolation threshold (see Fig. 7c and d). This indicates the presence of spin-dependent tunneling, i.e. in the "core–shell" nanogranules structure their oxidized shells play a role of insulating barriers for spin polarized current.

4. Discussion

Magnetometry of oxygen-free granular films reveals that values of saturation mass magnetization, M_S^{mass}, saturating field, H_S, and coercive field, H_C, corresponding to non-oxidized FeCoZr

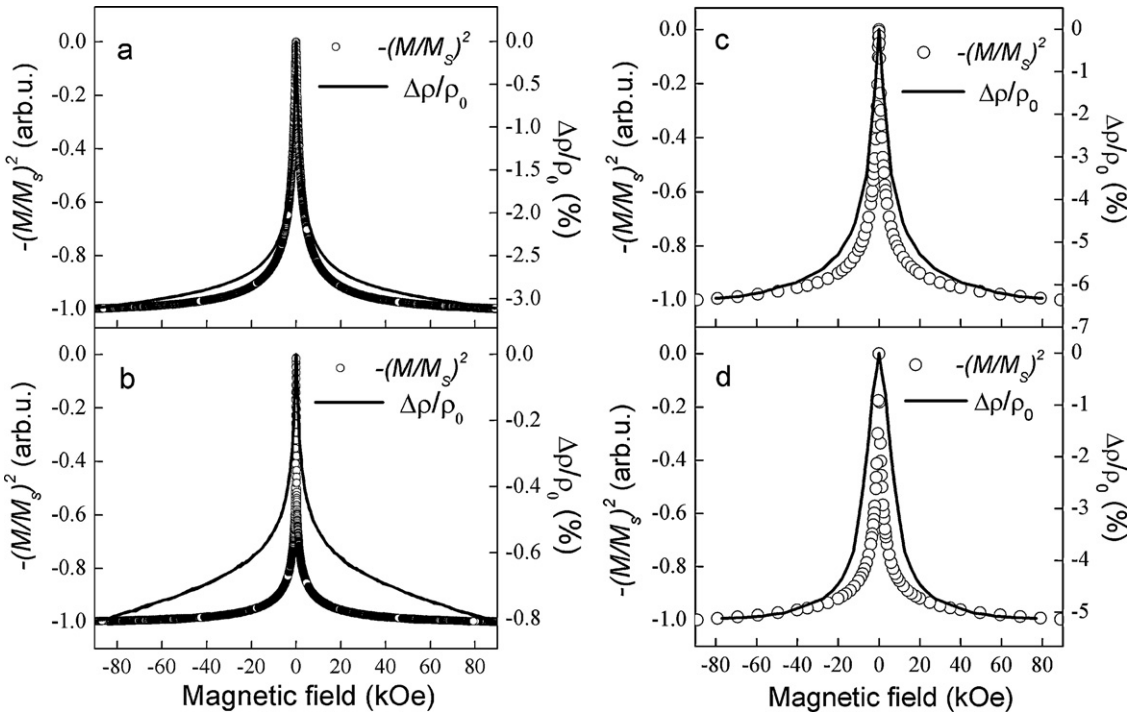

Fig. 7. $\Delta\rho/\rho$ and $-(M(H)/M_S)^2$ curves at 300 K for selected compositions FeCoZr-Al_2O_3: $(FeCoZr)_{42}(Al_2O_3)_{58}$ (a) and $(FeCoZr)_{47}(Al_2O_3)_{53}$ (b) sintered in oxygen-free atmosphere; $(FeCoZr)_{55}(Al_2O_3)_{45}$ (c) and $(FeCoZr)_{59}(Al_2O_3)_{41}$ (d) sintered in oxygen-containing sputtering atmosphere.

nanogranules are typical for amorphous metallic nanoparticles. Lower values of M_S^{mass} as compared to bulk Fe with crystalline structure reflect nanosized state of FeCoZr particles. Estimations presented in [11] and based on FC–ZFC curves confirmed that smaller FeCoZr nanoparticles are of 3–4 nm in size while larger nanogranules are of 7–9 nm in size.

Considering abovementioned Mössbauer spectroscopy results [8,9] the detected decrease of M_S^{mass} values in oxygen-containing granular films as compared to oxygen-free samples (see Table 1) can possibly be attributed to the formation of complex FeCo-containing oxides (including ferrites). It is known that M_S^{mass} values of bulk magnetite Fe_3O_4 and cobalt ferrite $CoFe_2O_4$ do not exceed 90 emu/g [15,16,20].

One should note that the results of magnetometry on granular films FeCoZr-Al_2O_3 synthesized in oxygen-containing sputtering atmosphere support the "core–shell" structure formation. It is consistent with non-saturating $M^{mass}(H)$ curves at 300 K, as this means that partially oxidized FeCoZr granules remain in superparamagnetic state even for compositions $(FeCoZr)_{56}(Al_2O_3)_{44}$ and $(FeCoZr)_{59}(Al_2O_3)_{41}$. Their superparamagnetic state correlates with mean diameter (6.5 nm and 5.7 nm) of oxidized nanogranules in $(FeCoZr)_{59}(Al_2O_3)_{41}$ film derived from Curie–Weiss relationship and from approximation of $M^{vol}(H)$ curves with Langevin function, respectively. Also the temperature dependence of coercive field $H_C(T)$ was typical for the ensemble of non-interacting magnetic nanoparticles. And, finally, spin-dependent tunneling for all compositions evidenced from a coincidence between $\Delta\rho/\rho$ and $-(M(H)/M_S)^2$ curves indirectly confirms that granular films studied contain superparamagnetic isolated nanogranules with «core-shell» structure. A deviation between $\Delta\rho/\rho$ and $-(M(H)/M_S)^2$ curves is expected to reflect percolation in granular films and formation of metallic conductivity path as it was observed in the case of samples synthesized in oxygen-free atmosphere.

It was mentioned above that H_C values for the sample $(FeCoZr)_{35}(Al_2O_3)_{65}$ were enhanced up to 889 Oe at 2 K as compared to $(FeCoZr)_{56}(Al_2O_3)_{44}$ and $(FeCoZr)_{59}(Al_2O_3)_{41}$ (H_C = 350 Oe, at 3 K). This is a typical behavior for oxygen-passivated metallic nanoparticles [21]. Moreover, a much larger value of the coercive field in oxidized $(FeCoZr)_{35}(Al_2O_3)_{65}$ granular film than for other films with higher FeCoZr content can be explained by the shape anisotropy model [17] which predicts an increase of H_C with decreasing packing fraction of magnetic particles.

H_C value for $(FeCoZr)_{35}(Al_2O_3)_{65}$ granular film sharply drops with increasing temperature and reaches zero value at T_B = 20–25 K. In fact, such a temperature dependence of H_C is expected as it reflects the increasing role of thermally activated fluctuations of magnetic moments of separate nanogranules with increasing temperature.

In addition, the low-temperature increase of coercive field in oxidized $(FeCoZr)_{35}(Al_2O_3)_{65}$ granular film may be considered in the context of coupling between antiferromagnetic (ferrimagnetic) (Fe^{3+})Co oxide shell and ferromagnetic FeCoZr core. In some papers [7] such an enhancement of H_C after FC procedure was assigned to AFM–FM coupling to weak unidirectional AFM anisotropy, even in the case when no shift of hysteresis loop was detected. In the case of weak AFM anisotropy, as evidenced in [7], spins of AFM shell are coupled with spins of FM cores and their coherent rotation is energetically more favorable. The additional energy originating from irreversible AFM spins turning results in the enhanced coercive force. It was also reported that AFM shell formation leads to the increased H_C values even after ZFC procedure. Some authors also assign the enhanced H_C in films with AFM–FM coupling to uniaxial exchange magnetic anisotropy [7]. Nevertheless, regardless of the origin of the enhancement, H_C values should vary after cooling in magnetic field and zero-magnetic field. However, this was not confirmed experimentally for $(FeCoZr)_{35}(Al_2O_3)_{65}$ granular film.

No signs of exchange AFM–FM coupling in the sample studied should be attributed to relatively low concentration of "core–shell" structures fully isolated in Al_2O_3 matrix. This conclusion correlates with previously published results on electrical conductivity [13], magnetoresistivity [13] and Mössbauer spectroscopy [8,9]. To some extend it is also confirmed with $M(T)$ dependencies obtained in FC–ZFC regimes revealing characteristic features of superparamagnetic nanoparticles (low T_B values, branching between ZFC- and FC curves). Similar behavior was reported for isolated Co nanoparticles in CoO shells where the absence of AFM-FM coupling was explained to be due to very small thickness of CoO layers or their highly disordered state [22].

Considering no significant effect of FC procedure at 2 K and $H = 80$ kOe on the H_C value and the hysteresis curve (i.e. no shift) the low-temperature enhancement of H_C, characterizing "core–shell" $(FeCoZr)_{35}(Al_2O_3)_{65}$ granular film could possibly be assigned to the pinning of the surface spins and their random canting within the interface between FeCoZr-(Fe^{3+})Co, (Fe^{2+})Co, or (Fe^{3+})Co, (Fe^{2+})Co-Al_2O_3 independently on the type of magnetic order in these interfaces. The resulting non-collinear structure related to such surface effect will be more pronounced for the smaller particle size [23,24].

5. Conclusions

Summarizing the results obtained, sputtering of complex target $FeCoZr + Al_2O_3$ in oxygen-containing atmosphere leads to the formation of heterogeneous composite structure containing nanogranules «FeCoZr core–(Fe^{3+})Co, (Fe^{2+})Co oxide shell» in Al_2O_3 matrix.

Decreased M_S^{mass} values, unsaturated character of $M^{mass}(H)$ curves at low temperatures, some peculiarities of $M(T)$, recorded in FC–ZFC regimes, as well as a good coincidence of field dependencies of magnetoresistivity and squared normalized magnetization support the picture of "ferromagnetic FeCoZr core–(Fe^{3+})Co, (Fe^{2+})Co oxide shell" structure.

No signature of exchange AFM-FM coupling between FeCoZr core and (Fe^{3+})Co, (Fe^{2+})Co) oxide shell in $(FeCoZr)_{35}(Al_2O_3)_{65}$ containing fully isolated "core–shell" nanogranules is found.

Enhanced coercive force H_C, that characterizes $(FeCoZr)_{35}(Al_2O_3)_{65}$ granular film at low temperature is assigned to the pinning effect of spins and their canting in the interfaces within the "core–shell" nanogranules independently on the type of magnetic ordering in the interfaces and the adjacent phases and/or to the shape anisotropy.

Appendix A. Supplementary data

Supplementary data associated with this article can be found, in the online version, at doi:10.1016/j.jallcom.2011.07.066.

References

[1] H.P. Khan, A. Granovsky, F. Brouers, E. Ganshina, J.P. Clerc, M. Kurmichev, J. Magn. Magn. Mater. 183 (1998) 127.
[2] L.B. Lutcev, Yu.E. Kalinin, A.V. Sitnikov, O.V. Stognej, Solid State Phys. 44 (2002) 1802 (in Russian).
[3] O.V. Stognej, A.V. Sitnikov, Yu.E. Kalinin, S.F. Avdeev, M.N. Kopytin, Solid State Phys. 49 (2007) 158 (in Russian).
[4] D. Stauffer, A. Aharony, Introduction to Percolation Theory, Taylor and Francis, London, 1992.
[5] D.L. Peng, K. Sumiyama, T.J. Konno, T. Hihara, S. Yamamuro, Phys. Rev. B 60 (4) (1999) 2093.
[6] M. Kovylina, M. Garcia del Muro, Z. Konstantinovich, M. Varela, O. Iglesias, A. Labarta, X. Batlle, Nanotechnology 20 (2009) 175702.
[7] J. Nogues, J. Sort, V. Langlais, V. Skumryev, S. Surinach, J.S. Munps, M.D. Baro, Phys. Rep. 422 (2005) 65.
[8] A. Saad, J. Fedotova, J. Nechaj, E. Szilagyi, M. Marszalek, J. Alloys Compd. 471 (1–2) (2009) 357.
[9] J. Fedotova, J. Kalinin, A. Fedotov, A. Sitnikov, I. Svito, A. Zaleski, A. Jablonska, Hyperfine Interact. 165 (2005) 127.
[10] I.V. Zolotukhin, Y.E. Kalinin, A.T. Ponomarenko, V.G. Shevchenko, A.V. Sitnikov, O.V. Stognei, O. Figovsky, J. Nanostruct. Polym. Nanocompos. 2 (2006) 23.
[11] M. Milosavljevich et al., unpublished results.
[12] J.A. Fedotova, FeCoZr-Al_2O_3 granular nanocomposite films with tailored structural, electric, magnetotransport and magnetic properties, in: B. Aktas, F. Mikailov (Eds.), Advances in Nanoscale Magnetism, Springer-Verlag, Berlin, 2008, p. 231.
[13] A. Saad, J. Kasiuk, J. Fedotova, E. Szilagyi, J. Przewoznik, Cz. Kapusta, M. Marszalek, Hyperfine Interact. 189 (2009) 111.
[14] T. Sourmail, Prog. Mater. Sci. 50 (2005) 816.
[15] H. Iida, K. Takayanagi, T. Nakanishi, T. Osaka, J. Colloids Interface Sci. 314 (2007) 274.
[16] P. Jeppson, R. Sailer, E. Jarabek, J. Sandstrom, B. Anderson, M. Bremer, D.G. Grier, D.L. Schulz, A.N. Caruso, S.A. Payne, P. Eames, M. Tondra, H. He, D.B. Chrisey, J. Appl. Phys. 100 (2006) 114324.
[17] B.D. Cullity, C.D. Graham, Introduction in Magnetic Materials, 2nd ed, Wiley/IEEE Press, Hoboken, 2009 (chapter 11).
[18] S. Giri, S. Samanta, S. Maji, S. Ganuli, A. Bhaumik, J. Magn. Magn. Mater. 285 (2005) 296.
[19] C. Wang, X. Xiao, Y. Rong, T.Y. Hsu, J. Mater. Sci. 41 (2006) 3873.
[20] O.V. Tolochko, D.W. Lee, C.J. Choi, D. Kim, M. Arif, Technical Phys. Lett. 31 (2005) 779.
[21] N.M. Dempsey, L. Ranno, D. Givord, J. Gonzalo, R. Serna, G.T. Fei, A.K. Petford-Long, R.C. Doole, D.E. Hole, J. Appl. Phys. 90 (2001) 6268.
[22] S.A. Koch, G. Palasantzas, T. Vystavel, J.Th.M. De Hosson, Phys. Rev. B 71 (2005) 085410–85411.
[23] R.H. Kodama, A.E. Berkowitz, E.J. McNiff Jr., S. Foner, Phys. Rev. Lett. 77 (1996) 394.
[24] H.M. Lu, W.T. Zheng, Q. Jiang, J. Phys. D: Appl. Phys. 40 (2007) 320.